

# Stability of superconducting gap symmetries arising from antiferromagnetic magnons

Chi Sun, Kristian Mæland, and Asle Sudbø\*

Center for Quantum Spintronics, Department of Physics, Norwegian University of Science and Technology, NO-7491 Trondheim, Norway

We consider a planar heterostructure consisting of a normal metal in proximity to an antiferromagnetic insulator, with an interlayer exchange-coupling between the metal and the insulator. The effective electron-electron interaction between electrons in the normal metal, mediated by antiferromagnetic magnons in the insulator, is derived to second order in the interlayer exchange coupling, using a Schrieffer-Wolff transformation. Particular emphasis is placed on including analytically derived expressions for the effective interactions including Umklapp processes in the solutions to the superconducting gap equation. The gap equation is first solved at the critical temperature as an eigenvalue problem by linearizing the gap equation. The eigenvectors yield information on the symmetry of the superconducting gap at the onset of superconductivity, and we derive a phase-diagram for the order-parameter in this case. In the various regimes of the phase-diagram, we find  $p$ -wave,  $f$ -wave, and  $d$ -wave superconductivity, with  $p$ -wave superconductivity in the dominant part of the phase diagram. Umklapp processes, that come into play with increasing size of the Fermi surface, yield  $f$ - and  $d$ -wave symmetries as the preferred symmetries when band filling approaches half-filling. To investigate the stability of this order parameter symmetry as the temperature is lowered, we also consider the nonlinear gap equation at zero temperature. We conclude that the phase diagram and the symmetries of the superconducting order parameter essentially are left intact as the temperature is lowered to zero temperature.

## I. INTRODUCTION

The interaction between a magnetic insulator (MI) and an adjacent nonmagnetic material forms a major research topic in the field of spintronics. Spin-orbit torque [1–3] and spin-pumping [4, 5] have been intensively studied to realize interconversion between electronic spin current in the nonmagnetic normal metal (NM) and magnonic spin current in the MI. Based on this, versatile electrically-manipulated devices [1] such as magnetic recording units [6], nano-oscillators [7–9] and domain-wall racetracks [10] are developed. In addition, it has been proposed that superconductivity can be introduced in MI/NM heterostructures [11–17]. Compared to conventional phonon-mediated superconductivity, the magnons in the MI are responsible for mediating an attractive interaction between the electrons in the neighboring NM, leading to the formation of a superconducting state. The magnon-mediated superconductivity has the potential to be enhanced by engineering the properties of the MI such as magnetic anisotropy [18] and magnon gap [12]. In addition, the MI/NM interface also plays a crucial role in manipulating the resulting superconductivity [13–16].

The ferromagnetic insulator (FMI) combines the advantages of ferromagnetism and insulators, which is highly needed for developing low dissipation spintronic devices [19, 20]. Based on FMI, magnon-mediated superconductivity has been proposed in a FMI/NM/FMI trilayer [11], in which a triplet  $p$ -wave superconducting pairing with critical temperature in the interval between 1–10 K is found. On the other hand, emerging research interests have recently been focused on antiferromagnetic insulators (AFMIs) with compensated magnetic moments, which possess a higher degree of stability and lower power consumption compared with FMIs [21, 22]. Similarly, it has been shown theoretically that an

electron-electron interaction yielding superconductivity can be mediated by antiferromagnetic magnons in an AFMI/NM bilayer [13] and an AFMI/NM/AFMI trilayer [12, 14]. In Refs. [13, 14] it is shown that asymmetric coupling to the sublattices of the AFMI gives rise to a potential enhancement of the critical temperature due to squeezing of magnons [23].

In the AFMI, magnons reside in a reduced Brillouin zone (RBZ) compared to the full Brillouin zone for electrons in the NM, which introduces electron-magnon scattering of two types, i.e., regular and Umklapp [see Fig. 1(b)]. The electrons are scattered with a momentum within the magnon RBZ through regular scattering. This is the only relevant process for small Fermi surfaces, like those considered in Ref. [13] for the AFMI/NM bilayer, where magnon-mediated  $p$ -wave superconductivity was found. In the Umklapp processes, the electrons are scattered out of the RBZ by receiving an additional momentum corresponding to a magnon lattice vector in the reciprocal space. This mechanism becomes important as the Fermi surface of the NM becomes larger and approaches half-filling, resulting in a  $d$ -wave phase based on the AFMI/NM/AFMI trilayer within a weak-coupling approach in Ref. [12] and within a strong-coupling approach in Ref. [14]. Ref. [14] also finds  $f$ -wave pairing close to half filling with sublattice coupling asymmetry.

In this work, we study magnon-mediated superconductivity in an AFMI/NM bilayer [see Fig. 1(a)] within a weak-coupling BCS framework, where both regular and Umklapp scatterings are treated on an equal footing. We analytically derive expressions for the effective electron-electron interactions mediated by magnons and numerically calculate the resulting nonlinear gap equation at zero temperature in addition to the critical temperature with the linearized gap equation. By modulating the asymmetry of interfacial sublattice exchange coupling and the chemical potential in the NM, the transition between different superconducting phases (i.e.,  $p$ -,  $d$ - and  $f$ -waves) are achieved. Our model provides both analytical and numerical insights into the AFMI magnon-mediated superconductivity, giving potential theoretical suggestions on how

\* Corresponding author: [asle.sudbo@ntnu.no](mailto:asle.sudbo@ntnu.no)

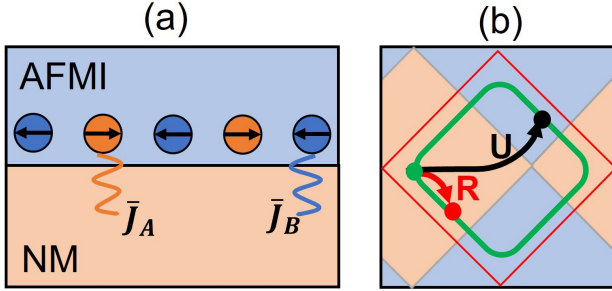


FIG. 1. (Color online) (a) Schematic representation of the bilayer structure considered in this paper, with a normal metal (NM) and an antiferromagnetic insulator (AFMI) on a bipartite lattice (orange and blue). The spins of the AFMI on the two sublattices interact with the spins of the electrons with exchange coupling constants that are allowed to be different on each sublattice, but are uniform within each sublattice. (b) Illustration of a regular (R) and Umklapp (U) scattering process. The entire square is the Brillouin zone for the electrons, while the red square illustrates the reduced magnetic Brillouin zone (RBZ). In a regular scattering process, magnons can transfer momenta  $\mathbf{q}$  between electrons in the range defined by the RBZ, i.e., within the orange region. Umklapp processes are necessary to reach momenta outside the RBZ, i.e., in the blue region.

to realize and manipulate magnon-mediated superconductivity experimentally.

## II. THEORY

### A. Model

The AFMI/NM bilayer system, illustrated in Fig. 1(a), is modeled by the Hamiltonian

$$H = H_{\text{AFMI}} + H_{\text{NM}} + H_{\text{int}}, \quad (1)$$

which consists of the AFMI, NM and interfacial terms whose explicit expressions are given by

$$H_{\text{AFMI}} = J \sum_{\langle i,j \rangle} \mathbf{S}_i \cdot \mathbf{S}_j - K \sum_i S_{iz}^2, \quad (2)$$

$$H_{\text{NM}} = -t \sum_{\langle i,j \rangle, \sigma} c_{i\sigma}^\dagger c_{j\sigma} - \mu \sum_{i,\sigma} c_{i\sigma}^\dagger c_{i\sigma}, \quad (3)$$

$$H_{\text{int}} = -2\bar{J}_A \sum_{i \in A} c_i^\dagger \boldsymbol{\sigma} c_i \cdot \mathbf{S}_i - 2\bar{J}_B \sum_{i \in B} c_i^\dagger \boldsymbol{\sigma} c_i \cdot \mathbf{S}_i. \quad (4)$$

Here the sum over  $\langle i,j \rangle$  includes all nearest neighboring sites. In the AFMI,  $J$  and  $K$  denote the antiferromagnetic exchange and easy-axis anisotropy (along  $\hat{z}$ ), respectively.  $\mathbf{S}_i$  is the spin operator at the lattice site  $i$ . In the NM,  $t$  is the tight-binding

hopping parameter and  $\mu$  represents the chemical potential.  $c_{i\sigma}^\dagger$  ( $c_{i\sigma}$ ) is the electron creation (annihilation) operator, which creates (annihilates) an electron with spin  $\sigma$  at site  $i$ . At the AFMI/NM interface,  $\bar{J}_A$  ( $\bar{J}_B$ ) parameterizes the sublattice-dependent interfacial exchange coupling. In the following, these interfacial strengths are described by the coupling asymmetry parameter  $\Omega \equiv \bar{J}_A/\bar{J}_B$  with  $\bar{J}_B \equiv \bar{J}$ . The notation  $c_i \equiv (c_{i\uparrow}, c_{i\downarrow})^T$  is introduced and  $\boldsymbol{\sigma}$  denotes the Pauli matrix vector in the spin space. In addition, we set  $\hbar = a = 1$ , where  $a$  is the lattice constant of the square lattice considered in this work.

Applying the Holstein-Primakoff and Fourier transformations for the two sublattice spin operators in the AFMI,  $H_{\text{AFMI}}$  is transferred into the momentum space in terms of the two individual sublattice magnons  $a_{\mathbf{q}}$  and  $b_{\mathbf{q}}$  (see Appendix A for details). Next, the Bogoliubov transformation with  $\alpha_{\mathbf{q}} = u_{\mathbf{q}} a_{\mathbf{q}} - v_{\mathbf{q}} b_{-\mathbf{q}}^\dagger$  and  $\beta_{\mathbf{q}} = u_{\mathbf{q}} b_{\mathbf{q}} - v_{\mathbf{q}} a_{-\mathbf{q}}^\dagger$  is performed to diagonalize the AFMI Hamiltonian, in which  $\alpha_{\mathbf{q}}$  and  $\beta_{\mathbf{q}}$  are the eigenmagnon operators defined as superpositions of  $a_{\mathbf{q}}$  and  $b_{\mathbf{q}}$ . The resulting diagonalized Hamiltonian is given by

$$H_{\text{AFMI}} = \sum_{\mathbf{q} \in \diamond} \omega_{\mathbf{q}} (\alpha_{\mathbf{q}}^\dagger \alpha_{\mathbf{q}} + \beta_{\mathbf{q}}^\dagger \beta_{\mathbf{q}}), \quad (5)$$

$$\omega_{\mathbf{q}} = 2s \sqrt{(zJ + K)^2 - z^2 J^2 \gamma_{\mathbf{q}}^2}, \quad (6)$$

in which  $\gamma_{\mathbf{q}} = (2/z)(\cos q_x + \cos q_y)$  is the structure factor.  $z$  and  $s$  are the number of nearest neighbors and spin quantum number, respectively.  $\diamond$  denotes summation over the RBZ. The coherence factors in the Bogoliubov transformation are obtained as  $u_{\mathbf{q}} = \cosh \theta_{\mathbf{q}}$  and  $v_{\mathbf{q}} = \sinh \theta_{\mathbf{q}}$  with  $\theta_{\mathbf{q}} = (1/2) \operatorname{artanh}[-Jz\gamma_{\mathbf{q}}/(zJ + K)]$ .

The NM Hamiltonian can be diagonalized as

$$H_{\text{NM}} = \sum_{\mathbf{k} \in \square, \sigma} \epsilon_{\mathbf{k}} c_{\mathbf{k}\sigma}^\dagger c_{\mathbf{k}\sigma}, \quad (7)$$

$$\epsilon_{\mathbf{k}} = -tz\gamma_{\mathbf{k}} - \mu, \quad (8)$$

in which  $\square$  denotes the sum over the full Brillouin zone. Here we utilized

$$\begin{aligned} c_{i\sigma} &= \frac{1}{\sqrt{N}} \sum_{\mathbf{k} \in \square} c_{\mathbf{k}\sigma} e^{-i\mathbf{k}\cdot\mathbf{r}_i} \\ &= \frac{1}{\sqrt{N}} \sum_{\mathbf{k} \in \diamond} (c_{\mathbf{k}\sigma} e^{-i\mathbf{k}\cdot\mathbf{r}_i} + c_{\mathbf{k}+\mathbf{G},\sigma} e^{-i(\mathbf{k}+\mathbf{G})\cdot\mathbf{r}_i}) \end{aligned} \quad (9)$$

in the Fourier transformation, where  $N$  is the number of lattice sites at the AFMI/NM interface.  $\mathbf{G} \equiv \pi(\hat{x} + \hat{y})$  is the reciprocal lattice vector, which occurs in the Umklapp scattering processes.

Utilizing the transformations shown in the Appendix A and Eq. (9), the interfacial Hamiltonian  $H_{\text{int}} = H_{\text{int}}^{(A)} + H_{\text{int}}^{(B)}$  is written in terms of diagonalized operators as

$$H_{\text{int}}^{(A)} = \Omega V \sum_{\mathbf{k} \in \square, \mathbf{q} \in \diamond} [(u_{\mathbf{q}} \alpha_{\mathbf{q}} + v_{\mathbf{q}} \beta_{-\mathbf{q}}^{\dagger})(c_{\mathbf{k}+\mathbf{q},\downarrow}^{\dagger} c_{\mathbf{k}\uparrow} + c_{\mathbf{k}+\mathbf{q}+\mathbf{G},\downarrow}^{\dagger} c_{\mathbf{k}\uparrow}) + (u_{\mathbf{q}} \alpha_{-\mathbf{q}}^{\dagger} + v_{\mathbf{q}} \beta_{\mathbf{q}})(c_{\mathbf{k}+\mathbf{q},\uparrow}^{\dagger} c_{\mathbf{k}\downarrow} + c_{\mathbf{k}+\mathbf{q}+\mathbf{G},\uparrow}^{\dagger} c_{\mathbf{k}\downarrow})], \quad (10)$$

$$H_{\text{int}}^{(B)} = V \sum_{\mathbf{k} \in \square, \mathbf{q} \in \diamond} [(u_{\mathbf{q}} \beta_{\mathbf{q}} + v_{\mathbf{q}} \alpha_{-\mathbf{q}}^{\dagger})(c_{\mathbf{k}+\mathbf{q},\uparrow}^{\dagger} c_{\mathbf{k}\downarrow} - c_{\mathbf{k}+\mathbf{q}+\mathbf{G},\uparrow}^{\dagger} c_{\mathbf{k}\downarrow}) + (u_{\mathbf{q}} \beta_{-\mathbf{q}}^{\dagger} + v_{\mathbf{q}} \alpha_{\mathbf{q}})(c_{\mathbf{k}+\mathbf{q},\downarrow}^{\dagger} c_{\mathbf{k}\uparrow} - c_{\mathbf{k}+\mathbf{q}+\mathbf{G},\downarrow}^{\dagger} c_{\mathbf{k}\uparrow})], \quad (11)$$

which couples the electrons in the NM with the A and B sublattice magnons in the AFMI. Here we define  $V \equiv -2\bar{J}\sqrt{s}/\sqrt{N}$ .

## B. Effective interaction

The full Hamiltonian of the AFMI/NM bilayer system can be written as  $H = H_0 + \eta H_1$ , in which we define

$$H_0 \equiv H_{\text{AFMI}} + H_{\text{NM}} = \sum_{\mathbf{q}} \omega_{\mathbf{q}} (\alpha_{\mathbf{q}}^{\dagger} \alpha_{\mathbf{q}} + \beta_{\mathbf{q}}^{\dagger} \beta_{\mathbf{q}}) + \sum_{\mathbf{k}\sigma} \epsilon_{\mathbf{k}} c_{\mathbf{k}\sigma}^{\dagger} c_{\mathbf{k}\sigma}, \quad (12)$$

$$\eta H_1 = \eta H_1^{(A)} + \eta H_1^{(B)} \equiv H_{\text{int}}^{(A)} + H_{\text{int}}^{(B)}. \quad (13)$$

In order to obtain an effective electron-electron interaction  $H_{\text{pair}}$  mediated by virtual magnons, we perform a canonical transformation by treating  $\eta H_1$  as a perturbation.  $\eta$  is a dummy-variable to count powers in the perturbation expansion. The resulting effective Hamiltonian takes the form of  $H_{\text{eff}} = H_0 + H_{\text{pair}}$  with (see Appendix B for details)

$$H_{\text{pair}} = \sum_{\mathbf{k}\mathbf{k}'} V_{\mathbf{k}\mathbf{k}'} c_{\mathbf{k}\uparrow}^{\dagger} c_{-\mathbf{k}\downarrow}^{\dagger} c_{-\mathbf{k}'\downarrow} c_{\mathbf{k}'\uparrow}, \quad (14)$$

in which

$$V_{\mathbf{k}\mathbf{k}'} = -V^2 \frac{2\omega_{\mathbf{q}}}{(\epsilon_{\mathbf{k}'} - \epsilon_{\mathbf{k}})^2 - \omega_{\mathbf{q}}^2} A(\mathbf{q}, \Omega), \quad (15)$$

$$A(\mathbf{q}, \Omega) = \frac{1}{2} (\Omega^2 + 1) (u_{\mathbf{q}}^2 + v_{\mathbf{q}}^2) + 2\Theta_{\mathbf{q}} \Omega u_{\mathbf{q}} v_{\mathbf{q}}, \quad (16)$$

$$\mathbf{q} = \begin{cases} \mathbf{k} + \mathbf{k}', & \mathbf{k} + \mathbf{k}' \in \diamond \\ \mathbf{k} + \mathbf{k}' + \mathbf{G}, & \mathbf{k} + \mathbf{k}' \notin \diamond \end{cases}, \quad (17)$$

$$\Theta_{\mathbf{q}} = \begin{cases} 1, & \mathbf{k} + \mathbf{k}' \in \diamond \\ -1, & \mathbf{k} + \mathbf{k}' \notin \diamond \end{cases}. \quad (18)$$

The effective interaction  $V_{\mathbf{k}\mathbf{k}'}$  in Eq. (18) is of the standard form well-known for electron-phonon interactions, apart from the factor  $A(\mathbf{q}, \Omega)$ . This is a factor that boosts the strength of the magnon-mediated electron-electron interaction. The boosting has two origins: i) Varying  $\Omega$  from 1 to 0 changes the combination of coherence factors in the interaction from  $(u_{\mathbf{q}} + v_{\mathbf{q}})^2$  to  $u_{\mathbf{q}}^2 + v_{\mathbf{q}}^2$ . Since  $u_{\mathbf{q}}$  and  $v_{\mathbf{q}}$  have opposite signs and tends to cancel for small  $\mathbf{q}$ , this vastly enhances the strength of the interaction for small-momenta scattering [13, 24]. ii) Umklapp scattering implies that the factor  $\Theta_{\mathbf{q}}$  takes on the opposite sign compared to regular scattering. Thus, even for

$\Omega = 1$  one obtains the combination  $(u_{\mathbf{q}} - v_{\mathbf{q}})^2$  instead of  $(u_{\mathbf{q}} + v_{\mathbf{q}})^2$ , again leading to a strengthening of the interaction [12, 13].

## III. RESULTS AND DISCUSSION

Consider the odd part of the pairing potential  $V_{\mathbf{k}\mathbf{k}'}^{O(\mathbf{k})} = \frac{1}{2}(V_{\mathbf{k}\mathbf{k}'} - V_{-\mathbf{k},\mathbf{k}'})$  for the  $S_z = 0$  spin triplet channel, i.e., the typical condensation channel for magnon-mediated superconductivity. The BCS gap function is defined as  $\Delta_{\mathbf{k}} = -\sum_{\mathbf{k}'} V_{\mathbf{k}\mathbf{k}'}^{O(\mathbf{k})} \langle c_{-\mathbf{k}'\uparrow} c_{\mathbf{k}'\downarrow} + c_{-\mathbf{k}'\downarrow} c_{\mathbf{k}'\uparrow} \rangle / 2$ . Within the standard weak-coupling mean-field theory approach [13, 25], the gap function becomes

$$\Delta_{\mathbf{k}} = -\sum_{\mathbf{k}'} V_{\mathbf{k}\mathbf{k}'}^{O(\mathbf{k})} \frac{\Delta_{\mathbf{k}'}}{2E_{\mathbf{k}'}} \tanh\left(\frac{E_{\mathbf{k}'}}{2k_B T}\right), \quad (19)$$

which is a nonlinear equation with respect to  $\Delta_{\mathbf{k}}$  with  $E_{\mathbf{k}} = \sqrt{\epsilon_{\mathbf{k}}^2 + |\Delta_{\mathbf{k}}|^2}$ . On the other hand, the even part of the pairing potential  $V_{\mathbf{k}\mathbf{k}'}^{E(\mathbf{k})} = \frac{1}{2}(V_{\mathbf{k}\mathbf{k}'} + V_{-\mathbf{k},\mathbf{k}'})$  corresponds to the spin singlet channel, where  $\Delta_{\mathbf{k}} = -\sum_{\mathbf{k}'} V_{\mathbf{k}\mathbf{k}'}^{E(\mathbf{k})} \langle c_{-\mathbf{k}'\uparrow} c_{\mathbf{k}'\downarrow} - c_{-\mathbf{k}'\downarrow} c_{\mathbf{k}'\uparrow} \rangle / 2$ . Its gap equation takes the same form as Eq. (19), except that  $V_{\mathbf{k}\mathbf{k}'}^{O(\mathbf{k})}$  is replaced by  $V_{\mathbf{k}\mathbf{k}'}^{E(\mathbf{k})}$ .

### A. Gap equation at critical temperature

When the temperature  $T$  approaches its critical value  $T_c$  from below, the magnitude of  $\Delta_{\mathbf{k}}$  in  $E_{\mathbf{k}} = \sqrt{\epsilon_{\mathbf{k}}^2 + |\Delta_{\mathbf{k}}|^2}$  can be treated as negligible, giving rise to a linearized gap equation

$$\Delta_{\mathbf{k}} = -\sum_{\mathbf{k}'} V_{\mathbf{k}\mathbf{k}'}^{O(\mathbf{k})} \frac{\Delta_{\mathbf{k}'}}{2|\epsilon_{\mathbf{k}'}|} \tanh\left(\frac{|\epsilon_{\mathbf{k}'}|}{2k_B T_c}\right). \quad (20)$$

In the following, we assume that the gap is nonzero only close to the Fermi surface for momenta such that  $|\epsilon_{\mathbf{k}}|, |\epsilon_{\mathbf{k}'}| < \omega_c$ , with  $\omega_c = 2szJ$  the magnon cutoff energy at the Brillouin zone boundary. Furthermore,  $\tanh(|\epsilon_{\mathbf{k}'}|/2k_B T_c)/2|\epsilon_{\mathbf{k}'}|$  is peaked at the Fermi surface, justifying a Fermi surface average [25],

$$\Delta_{\mathbf{k}} = -D(\mu) \langle V_{\mathbf{k}\mathbf{k}'}^{O(\mathbf{k})} \Delta_{\mathbf{k}'} \rangle_{\mathbf{k}', \text{FS}} \int_{-\omega_c}^{\omega_c} d\epsilon \frac{1}{2|\epsilon|} \tanh\left(\frac{|\epsilon|}{2k_B T_c}\right), \quad (21)$$

where  $D(\mu)$  is the density of states per spin on the Fermi surface (see Appendix C for its explicit expression) and  $\langle \rangle_{\mathbf{k}', \text{FS}}$

denotes the angular average over the Fermi surface. Next, a dimensionless coupling constant is defined as [26]

$$\frac{1}{\lambda} = \int_{-\omega_c}^{\omega_c} d\epsilon \frac{1}{2|\epsilon|} \tanh\left(\frac{|\epsilon|}{2k_B T_c}\right) \approx \ln\left(\frac{1.13\omega_c}{k_B T_c}\right), \quad (22)$$

in which the weak-coupling limit ( $\lambda \ll 1$ ) is assumed. In terms of  $\lambda$ , the gap function can be written as

$$\lambda \Delta_{\mathbf{k}} = -D(\mu) \langle V_{\mathbf{k}\mathbf{k}'}^{O(\mathbf{k})} \Delta_{\mathbf{k}'} \rangle_{\mathbf{k}',\text{FS}}, \quad (23)$$

which becomes an eigenvalue problem by picking discrete points equidistantly placed on the Fermi surface for  $\mathbf{k}$  and  $\mathbf{k}'$  to construct  $V_{\mathbf{k}\mathbf{k}'}^{O(\mathbf{k})}$  as a matrix. Consequently,  $\lambda$  and  $\Delta_{\mathbf{k}}$  can be solved as eigenvalues and eigenvectors, respectively. Here we utilize the largest eigenvalue for  $\lambda$  to determine  $T_c$  and its corresponding eigenvector to get the gap structure information. While this procedure determines  $T_c$ , it only determines the gap-amplitude up to a multiplicative constant. We will return to this below when we consider solutions to the gap equation for  $T < T_c$ . Based on Eq. (22), the estimated critical temperature  $T_c$  is given by

$$k_B T_c = \frac{2e^\gamma}{\pi} \omega_c e^{-1/\lambda} \approx 1.13\omega_c e^{-1/\lambda}, \quad (24)$$

where  $\gamma = 0.577\ldots$  is Euler's constant. As described above, we follow the same procedure to obtain  $T_c$  for the spin singlet channel with  $V_{\mathbf{k}\mathbf{k}'}^{E(\mathbf{k})}$  and then determine the final  $T_c$  as the greatest value obtained from these two channels. Employing plausible material parameters obtained from experiments [12, 13, 27, 28], the critical temperature  $T_c$  is plotted as a phase diagram in terms of the chemical potential  $\mu$  and the asymmetry parameter  $\Omega \equiv \bar{J}_A/\bar{J}_B$  in Fig. 2, where different colors are utilized to show the symmetries of their corresponding gaps (i.e., eigenvectors). In the green region with smaller  $\mu$  and  $\Omega$ , we find spin triplet  $p$ -wave superconductivity. Specifically, we find nodal and topologically trivial  $p_x$ - or  $p_y$ -wave solutions which we refer to as  $p$ -wave. Our definitions of gap symmetries follow conventional notation and the relevant symmetries are illustrated in Ref. [14].

In the  $p$ -wave region the highest  $T_c \sim 50$  K is achieved at the largest asymmetry  $\Omega = 0$  and the lowest chemical potential  $\mu = -3.9t$ . At such low filling, the Fermi surface is small, ensuring that all scattering processes involve small magnitudes of magnon momenta  $\mathbf{q}$  where the strongest coupling is expected for small  $\Omega$  [13, 24]. A similar increase in  $T_c$  for small Fermi surfaces and small  $\Omega$  was found within a strong-coupling calculation in Ref. [14]. Lower  $\mu$  corresponds to smaller Fermi surfaces, which ensures that the scattering processes between points on the Fermi surfaces are of the regular type. As  $\mu$  increases, the Fermi surface becomes larger and approaches half filling such that Umklapp processes are required to cover any point on the Fermi surface from a Fermi surface starting point. This gives rise to  $f$ -wave superconductivity in the spin triplet channel, as shown by the blue region. On the other hand, spin-singlet  $d$ -wave superconductivity has a higher  $T_c$  than the  $f$ -wave phase in the spin-triplet channel

for higher  $\mu$  and larger values of  $\Omega$ , which results in the red region in Fig. 2.

Similar phase transitions can also be achieved based on the strong-coupling Eliashberg theory [14]. This is an important point, since the boosting mechanism for  $T_c$ , involving both Umklapp and the coherence factors from diagonalizing the antiferromagnetic magnons, easily puts us in the strong-coupling regime. Ref. [14] finds an effective cutoff on the magnon spectrum that is lower than  $\omega_c = 2szJ$ , giving a reduction of the estimated  $T_c$ . The similarity of our present results to the strong-coupling results as far as the symmetry of the gap is concerned right at  $T = T_c$ , motivates us to also consider the low-temperature limit. This problem is considerably more demanding numerically, since the equations to be solved are non-linear.

## B. Gap equation at zero temperature

To investigate the low temperature behavior of the superconductor, we consider the gap equation at zero temperature. The main purpose of this is to investigate if the symmetry of the superconducting order parameter that we find at  $T = T_c$  is altered in any significant way as the temperature is lowered. To investigate the low-temperature regime, we consider the limit  $T = 0$ , since we expect the temperature-dependence of the gap to saturate well above  $T = 0$ . The present analysis therefore extends previous work using weak-coupling BCS-theory not including Umklapp, where only the  $T = T_c$  case was studied in Ref. [13]. It also extends the work properly including Umklapp-processes [14], which only considered  $T = T_c$ .

Applying the Fermi surface average in the nonlinear Eq. (19), the ensuing gap takes the form

$$\Delta_{\mathbf{k}} = -D(\mu) \langle V_{\mathbf{k}\mathbf{k}'}^{O(\mathbf{k})} \Delta_{\mathbf{k}'} \chi(\Delta_{\mathbf{k}'}) \rangle_{\mathbf{k}',\text{FS}} \quad (25)$$

where

$$\chi(\Delta_{\mathbf{k}'}) = \int_{-\omega_c}^{\omega_c} d\epsilon \frac{\tanh\left(\sqrt{\epsilon^2 + |\Delta_{\mathbf{k}'}|^2}/2k_B T\right)}{2\sqrt{\epsilon^2 + |\Delta_{\mathbf{k}'}|^2}}. \quad (26)$$

Using  $\tanh\left(\sqrt{\epsilon^2 + |\Delta_{\mathbf{k}'}|^2}/2k_B T\right) \rightarrow 1$  at  $T = 0$ , we obtain the analytical expression

$$\chi(\Delta_{\mathbf{k}'}) = \int_0^{\omega_c} \frac{d\epsilon}{\sqrt{\epsilon^2 + \Delta_{\mathbf{k}'}^2}} = \text{arsinh}\left(\frac{\omega_c}{|\Delta_{\mathbf{k}'}|}\right). \quad (27)$$

Next, we insert the gap information obtained at  $T_c$  in the previous section to construct a trial solution in order to numerically solve the nonlinear Eq. (25) at zero temperature.  $\Delta_{\text{max}}(0)$  is defined as the largest amplitude of the gap function at zero temperature of the spin singlet and triplet channels. The amplitude of the trial solution is set to  $2\omega_c e^{-1/\lambda}$  based on the BCS result for the zero temperature gap amplitude [26]. Fig. 3 is the resulting phase diagram for  $\Delta_{\text{max}}(0)$ , which shows almost the same superconducting symmetries as Fig. 2

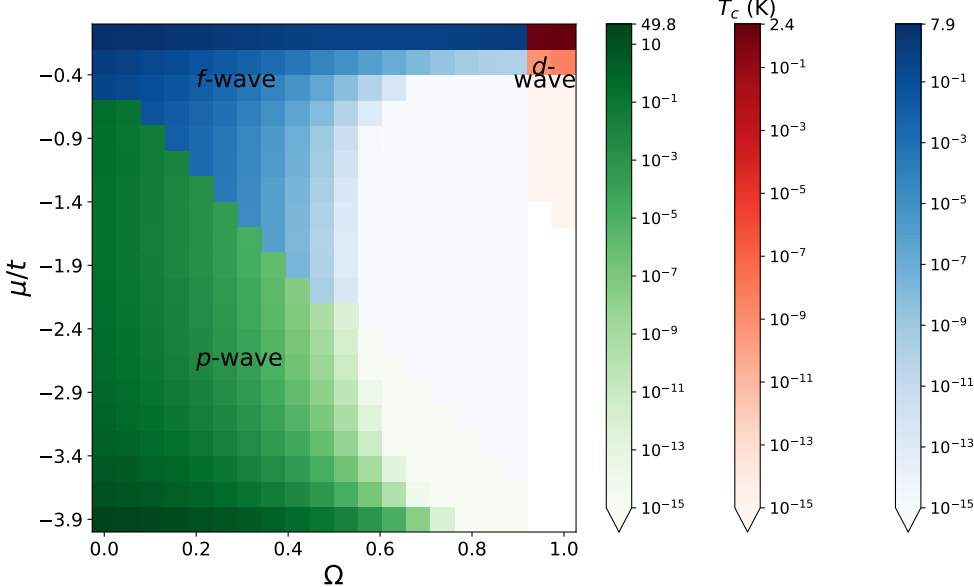


FIG. 2. (Color online) Phase diagram of the critical temperature  $T_c$  in terms of sublattice coupling asymmetry  $\Omega$  and chemical potential  $\mu$ . The green, blue and red colors correspond to spin-triplet  $p$ -wave, spin-triplet  $f$ -wave, and spin singlet  $d$ -wave phases, respectively. Here, we have used parameter values  $J = 5$  meV,  $K = J/2000$ ,  $\bar{J} = 20$  meV,  $s = 1$ ,  $z = 4$  and  $t = 1$  eV.

at the critical temperature except for small differences at the transition boundaries. Close to the phase boundaries we considered both symmetries found at  $T = T_c$  for the trial solution and found that only one symmetry converged at each point in the  $(\mu, \Omega)$ -phase diagram with the chosen resolution.

#### IV. CONCLUSION

In this paper, we have considered superconducting ordering mediated by antiferromagnetic magnons both close to the critical temperature and in the low-temperature regime. We use a BCS weak-coupling approach with an effective magnon-mediated electron-electron interaction. Specifically, we have utilized analytical expressions for effective interactions mediated by such magnons, including properly the effect of Umklapp-processes, which will be important once the Fermi-surface is large enough that any two points on the Fermi surface cannot be connected by the momenta of the magnetic Brillouin-zone, available to the magnons. We find that Umklapp processes play an important role in determining the correct superconducting gap-symmetry over large tracts of the  $(\mu, \Omega)$ -phase diagram. At low to intermediate filling fractions, we find  $p$ -wave pairing, while for most values of  $\Omega$  we find  $f$ -wave pairing for intermediate to large filling fractions. Close to  $\Omega = 1$ , we find  $d$ -wave pairing. The results obtained at  $T = T_c$  correspond well to the results obtained at  $T = 0$ . Hence, the symmetries found for the superconducting gap-function are stable to variation in temperature. Our results at  $T = T_c$  obtained within a BCS weak-coupling approach are in very good agreement with previous results found using a

much more elaborate strong-coupling Eliashberg-Migdal approach.

#### ACKNOWLEDGMENTS

We acknowledge funding from the Research Council of Norway (RCN) through its Centres of Excellence funding scheme, Project No. 262633, “QuSpin,” and RCN through Project No. 323766, “Equilibrium and out-of-equilibrium quantum phenomena in superconducting hybrids with antiferromagnets and topological insulators.”

#### Appendix A: Holstein-Primakoff and Fourier transformations

We introduce the Holstein-Primakoff transformation for the two sublattice spin operators in the AFMI

$$S_{i+}^A = S_{ix}^A + iS_{iy}^A = \sqrt{2s - a_i^\dagger a_i} \approx \sqrt{2s} a_i, \quad (A1)$$

$$S_{i-}^A = S_{ix}^A - iS_{iy}^A = a_i^\dagger \sqrt{2s - a_i^\dagger a_i} \approx \sqrt{2s} a_i^\dagger, \quad (A2)$$

$$S_{iz}^A = s - a_i^\dagger a_i, \quad (A3)$$

$$S_{j+}^B = S_{jx}^B + iS_{jy}^B = b_j^\dagger \sqrt{2s - b_j^\dagger b_j} \approx \sqrt{2s} b_j^\dagger, \quad (A4)$$

$$S_{j-}^B = S_{jx}^B - iS_{jy}^B = \sqrt{2s - b_j^\dagger b_j} b_j \approx \sqrt{2s} b_j, \quad (A5)$$

$$S_{jz}^B = -s + b_j^\dagger b_j, \quad (A6)$$

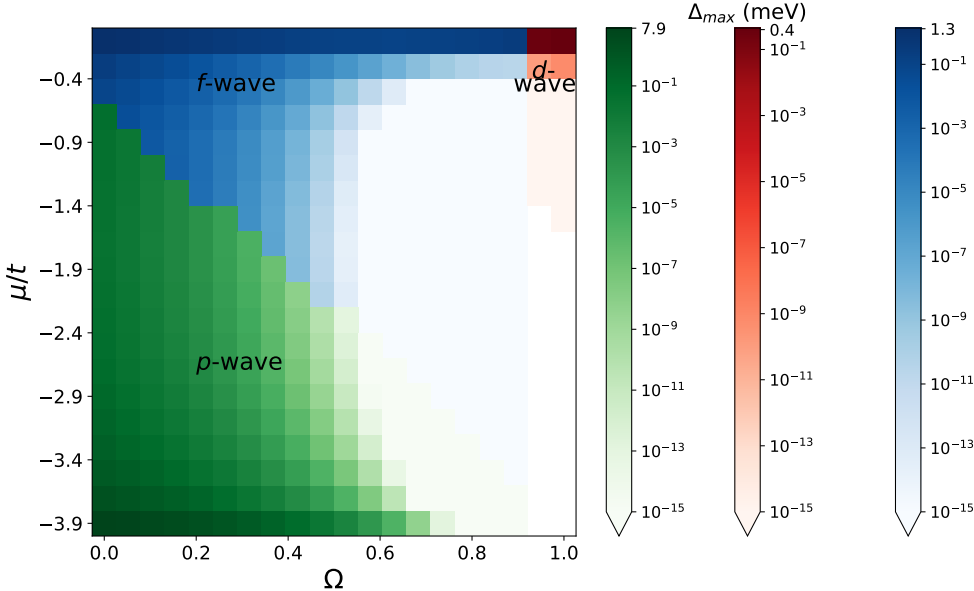


FIG. 3. (Color online) Phase diagram of the gap maximum  $\Delta_{\max}$  at zero temperature in terms of sublattice coupling asymmetry  $\Omega$  and chemical potential  $\mu$ . The green, blue and red colors correspond to the spin-triplet  $p$ -wave, spin-triplet  $f$ -wave and spin singlet  $d$ -wave phases, respectively. Here we use the same parameters as indicated for Fig. 2.

where  $a_i$  and  $b_j$  are the two sublattice magnon operators and  $s$  is the spin quantum number associated with the lattice site spins. Next, we perform the Fourier transformations of the magnon operators

$$a_i = \frac{1}{\sqrt{N_A}} \sum_{\mathbf{q} \in \diamond} a_{\mathbf{q}} e^{-i\mathbf{q} \cdot \mathbf{r}_i}, \quad b_i = \frac{1}{\sqrt{N_B}} \sum_{\mathbf{q} \in \diamond} b_{\mathbf{q}} e^{-i\mathbf{q} \cdot \mathbf{r}_i}, \quad (A7)$$

in which  $N_A = N_B = N/2$  and  $N$  is the number of lattice sites at the AFMI/NM interface.  $\diamond$  is used to mark the sum over the RBZ.

Inserting these transformations directly in  $H_{\text{int}}$  yields some additional terms that have been ignored compared to Eqs. (10) and (11). First, terms involving two magnon operators are assumed negligible compared to the one-magnon processes. Second, terms involving only electron operators, akin to Zeeman terms, are expected to have little influence on our results [13]. They are only nonzero for  $\Omega < 1$ , and can be eliminated

by considering an AFMI/NM/AFMI trilayer [14].

## Appendix B: Derivation of effective interaction

Here we derive the effective interaction mediated by the antiferromagnetic magnons. We use a Schrieffer-Wolff transformation to obtain an effective magnon-mediated interaction to second order in the coupling constant  $\bar{J}$  between the AFMI and the electron spins in the NM. This is effectuated by a canonical transformation  $H' = e^{-\eta S} H e^{\eta S}$ , such that the pairing interaction to second order in  $V \equiv -2\bar{J}\sqrt{s}/\sqrt{N}$  becomes

$$H_{\text{pair}} = \sum_{LL'} H_{\text{pair}}^{(L,L')} = \sum_{LL'} \frac{1}{2} [\eta H_1^{(L)}, \eta S^{(L')}], \quad (B1)$$

where  $L \in \{A, B\}$  and  $\eta S^{(L)}$  satisfies

$$\eta H_1^{(L)} + [H_0, \eta S^{(L)}] = 0. \quad (B2)$$

Choosing the ansatze

$$\begin{aligned} \eta S^{(A)} = \Omega V \sum_{\mathbf{k}\mathbf{q}} & [(x_{\mathbf{k},\mathbf{q}} u_{\mathbf{q}} \alpha_{\mathbf{q}} + y_{\mathbf{k},\mathbf{q}} v_{\mathbf{q}} \beta_{-\mathbf{q}}^\dagger) c_{\mathbf{k}+\mathbf{q},\downarrow}^\dagger c_{\mathbf{k}\uparrow} + (x_{\mathbf{k},\mathbf{q},\mathbf{G}} u_{\mathbf{q}} \alpha_{\mathbf{q}} + y_{\mathbf{k},\mathbf{q},\mathbf{G}} v_{\mathbf{q}} \beta_{-\mathbf{q}}^\dagger) c_{\mathbf{k}+\mathbf{q}+\mathbf{G},\downarrow}^\dagger c_{\mathbf{k}\uparrow} \\ & + (z_{\mathbf{k},\mathbf{q}} u_{\mathbf{q}} \alpha_{-\mathbf{q}}^\dagger + w_{\mathbf{k},\mathbf{q}} v_{\mathbf{q}} \beta_{\mathbf{q}}) c_{\mathbf{k}+\mathbf{q},\uparrow}^\dagger c_{\mathbf{k}\downarrow} + (z_{\mathbf{k},\mathbf{q},\mathbf{G}} u_{\mathbf{q}} \alpha_{-\mathbf{q}}^\dagger + w_{\mathbf{k},\mathbf{q},\mathbf{G}} v_{\mathbf{q}} \beta_{\mathbf{q}}) c_{\mathbf{k}+\mathbf{q}+\mathbf{G},\uparrow}^\dagger c_{\mathbf{k}\downarrow}], \end{aligned} \quad (B3)$$

$$\begin{aligned} \eta S^{(B)} = V \sum_{\mathbf{k}, \mathbf{q}} & [(w_{\mathbf{k}, \mathbf{q}} u_{\mathbf{q}} \beta_{\mathbf{q}} + z_{\mathbf{k}, \mathbf{q}} v_{\mathbf{q}} \alpha_{-\mathbf{q}}^\dagger) c_{\mathbf{k}+\mathbf{q}, \uparrow}^\dagger c_{\mathbf{k} \downarrow} - (w_{\mathbf{k}, \mathbf{q}, \mathbf{G}} u_{\mathbf{q}} \beta_{\mathbf{q}} + z_{\mathbf{k}, \mathbf{q}, \mathbf{G}} v_{\mathbf{q}} \alpha_{-\mathbf{q}}^\dagger) c_{\mathbf{k}+\mathbf{q}+\mathbf{G}, \uparrow}^\dagger c_{\mathbf{k} \downarrow} \\ & + (y_{\mathbf{k}, \mathbf{q}} u_{\mathbf{q}} \beta_{-\mathbf{q}}^\dagger + x_{\mathbf{k}, \mathbf{q}} v_{\mathbf{q}} \alpha_{\mathbf{q}}) c_{\mathbf{k}+\mathbf{q}, \downarrow}^\dagger c_{\mathbf{k} \uparrow} - (y_{\mathbf{k}, \mathbf{q}, \mathbf{G}} u_{\mathbf{q}} \beta_{-\mathbf{q}}^\dagger + x_{\mathbf{k}, \mathbf{q}, \mathbf{G}} v_{\mathbf{q}} \alpha_{\mathbf{q}}) c_{\mathbf{k}+\mathbf{q}+\mathbf{G}, \downarrow}^\dagger c_{\mathbf{k} \uparrow}], \end{aligned} \quad (\text{B4})$$

and inserting them into Eq. (B2), the coefficients in the ansatze can be solved as

$$x_{\mathbf{k}, \mathbf{q}} = w_{\mathbf{k}, \mathbf{q}} = \frac{1}{\epsilon_{\mathbf{k}} - \epsilon_{\mathbf{k}+\mathbf{q}} + \omega_{\mathbf{q}}}, \quad (\text{B5})$$

$$y_{\mathbf{k}, \mathbf{q}} = z_{\mathbf{k}, \mathbf{q}} = \frac{1}{\epsilon_{\mathbf{k}} - \epsilon_{\mathbf{k}+\mathbf{q}} - \omega_{\mathbf{q}}}, \quad (\text{B6})$$

Given  $\eta S^{(L)}$ , the pairing effective electron-electron interactions given by Eq. (B1) are calculated as

$$\begin{aligned} H_{\text{pair}}^{(A, A)} = \frac{1}{2} \Omega^2 V^2 \sum_{\mathbf{k}, \mathbf{k}' \mathbf{q}} & \{ [u_{\mathbf{q}}^2 (y_{\mathbf{k}', -\mathbf{q}} - x_{\mathbf{k}, \mathbf{q}}) + v_{\mathbf{q}}^2 (y_{\mathbf{k}, \mathbf{q}} - x_{\mathbf{k}', -\mathbf{q}})] c_{\mathbf{k}+\mathbf{q}, \downarrow}^\dagger c_{\mathbf{k} \uparrow} c_{\mathbf{k}' - \mathbf{q}, \uparrow}^\dagger c_{\mathbf{k}' \downarrow} \\ & + [u_{\mathbf{q}}^2 (y_{\mathbf{k}', -\mathbf{q}, \mathbf{G}} - x_{\mathbf{k}, \mathbf{q}, \mathbf{G}}) + v_{\mathbf{q}}^2 (y_{\mathbf{k}, \mathbf{q}, \mathbf{G}} - x_{\mathbf{k}', -\mathbf{q}, \mathbf{G}})] c_{\mathbf{k}+\mathbf{q}+\mathbf{G}, \downarrow}^\dagger c_{\mathbf{k} \uparrow} c_{\mathbf{k}' - \mathbf{q}+\mathbf{G}, \uparrow}^\dagger c_{\mathbf{k}' \downarrow} \}, \end{aligned} \quad (\text{B7})$$

$$\begin{aligned} H_{\text{pair}}^{(B, B)} = \frac{1}{2} V^2 \sum_{\mathbf{k}, \mathbf{k}' \mathbf{q}} & \{ [u_{\mathbf{q}}^2 (y_{\mathbf{k}, \mathbf{q}} - x_{\mathbf{k}', -\mathbf{q}}) + v_{\mathbf{q}}^2 (y_{\mathbf{k}', -\mathbf{q}} - x_{\mathbf{k}, \mathbf{q}})] c_{\mathbf{k}+\mathbf{q}, \downarrow}^\dagger c_{\mathbf{k} \uparrow} c_{\mathbf{k}' - \mathbf{q}, \uparrow}^\dagger c_{\mathbf{k}' \downarrow} \\ & + [u_{\mathbf{q}}^2 (y_{\mathbf{k}, \mathbf{q}, \mathbf{G}} - x_{\mathbf{k}', -\mathbf{q}, \mathbf{G}}) + v_{\mathbf{q}}^2 (y_{\mathbf{k}', -\mathbf{q}, \mathbf{G}} - x_{\mathbf{k}, \mathbf{q}, \mathbf{G}})] c_{\mathbf{k}+\mathbf{q}+\mathbf{G}, \downarrow}^\dagger c_{\mathbf{k} \uparrow} c_{\mathbf{k}' - \mathbf{q}+\mathbf{G}, \uparrow}^\dagger c_{\mathbf{k}' \downarrow} \}, \end{aligned} \quad (\text{B8})$$

$$\begin{aligned} H_{\text{pair}}^{(A, B)} + H_{\text{pair}}^{(B, A)} = \Omega V^2 \sum_{\mathbf{k}, \mathbf{k}' \mathbf{q}} & [u_{\mathbf{q}} v_{\mathbf{q}} (y_{\mathbf{k}, \mathbf{q}} + y_{\mathbf{k}', -\mathbf{q}} - x_{\mathbf{k}, \mathbf{q}} - x_{\mathbf{k}', -\mathbf{q}}) c_{\mathbf{k}+\mathbf{q}, \downarrow}^\dagger c_{\mathbf{k} \uparrow} c_{\mathbf{k}' - \mathbf{q}, \uparrow}^\dagger c_{\mathbf{k}' \downarrow} \\ & - u_{\mathbf{q}} v_{\mathbf{q}} (y_{\mathbf{k}, \mathbf{q}, \mathbf{G}} + y_{\mathbf{k}', -\mathbf{q}, \mathbf{G}} - x_{\mathbf{k}, \mathbf{q}, \mathbf{G}} - x_{\mathbf{k}', -\mathbf{q}, \mathbf{G}}) c_{\mathbf{k}+\mathbf{q}+\mathbf{G}, \downarrow}^\dagger c_{\mathbf{k} \uparrow} c_{\mathbf{k}' - \mathbf{q}+\mathbf{G}, \uparrow}^\dagger c_{\mathbf{k}' \downarrow}]. \end{aligned} \quad (\text{B9})$$

We next assume that only electrons with opposite momenta interact. Inserting the expressions in Eqs. (B5-B6), we then obtain the effective electron-electron interaction for scattering electron-pairs from  $(\mathbf{k}', -\mathbf{k}')$  to  $(\mathbf{k}, -\mathbf{k})$ , given in Eq. (14).

### Appendix C: Density of states in the NM

Following Refs. [15, 29], the density of states per spin in the NM can be calculated as

$$D(\epsilon) = \sum_{\mathbf{k} \in \square} \delta(\epsilon - \epsilon_{\mathbf{k}}) = \frac{N}{A_{\square}} \int_{-\pi}^{\pi} d\theta \int_0^{c(\theta)} dk k \delta(\epsilon - \epsilon_{\mathbf{k}, \theta}), \quad (\text{C1})$$

in which  $\theta = \text{atan}2(k_y/k_x)$  with  $k_x = k \cos \theta$  and  $k_y = k \sin \theta$ .  $A_{\square} = 4\pi^2$  denotes the area of the full Brillouin zone

$\square$  and the upper cutoff  $c(\theta) = \pi / \max\{|\cos \theta|, |\sin \theta|\}$  confines the integral to  $\mathbf{k} \in \square$ .

Given a function  $f(k)$  with roots  $k_i$  and  $f'(k_i) \neq 0$ ,  $\delta[f(k)] = \sum_i \delta(k - k_i) / |f'(k_i)|$ . Here we have  $f(k) = \epsilon + 2t[\cos(k \cos \theta) + \cos(k \sin \theta)]$  based on Eq. (8) with  $\mu = 0$ . Consequently, we have

$$D(\epsilon) = \frac{N}{A_{\square}} \int_{-\pi}^{\pi} d\theta \sum_i \frac{k_i(\theta)}{|f'[k_i(\theta)]|}. \quad (\text{C2})$$

Since  $\epsilon$  and  $\mu$  enter the above equations in the same way, we can use Eq. (C2) from setting  $\mu = 0$  to obtain the density of states on the Fermi surface ( $\epsilon = 0$ ) at nonzero  $\mu$  as  $D(\epsilon = \mu) \equiv D(\mu)$ .

---

[1] Q. Shao, P. Li, L. Liu, H. Yang, S. Fukami, A. Razavi, H. Wu, K. Wang, F. Freimuth, Y. Mokrousov, M. D. Stiles, S. Emori, A. Hoffmann, J. Åkerman, K. Roy, J.-P. Wang, S.-H. Yang, K. Garello, and W. Zhang, *IEEE Trans. Magn.* **57**, 1 (2021).

[2] R. Ramaswamy, J. M. Lee, K. Cai, and H. Yang, *Appl. Phys. Rev.* **5**, 031107 (2018).

[3] P. Gambardella and I. M. Miron, *Philos. Trans. Royal Soc. A* **369**, 3175 (2011).

[4] B. Heinrich, C. Burrowes, E. Montoya, B. Kardasz, E. Girt, Y.-Y. Song, Y. Sun, and M. Wu, *Phys. Rev. Lett.* **107**, 066604 (2011).

[5] R. Cheng, J. Xiao, Q. Niu, and A. Brataas, *Phys. Rev. Lett.* **113**,

057601 (2014).

[6] C. O. Avci, A. Quindeau, C.-F. Pai, M. Mann, L. Caretta, A. S. Tang, M. C. Onbasli, C. A. Ross, and G. S. D. Beach, *Nat. Mater.* **16**, 309 (2017).

[7] T. Chen, R. K. Dumas, A. Eklund, P. K. Muduli, A. Houshang, A. A. Awad, P. Dürrenfeld, B. G. Malm, A. Rusu, and J. Åkerman, *Proc. IEEE* **104**, 1919 (2016).

[8] M. Collet, X. de Milly, O. D'Allivy Kelly, V. V. Naletov, R. Bernard, P. Bortolotti, J. Ben Youssef, V. E. Demidov, S. O. Demokritov, J. L. Prieto, M. Muñoz, V. Cros, A. Anane, G. de Loubens, and O. Klein, *Nat. Commun.* **7**, 1 (2016).

[9] M. Evelt, C. Safranski, M. Aldosary, V. E. Demidov, I. Barusukov, A. P. Nosov, A. B. Rinkevich, K. Sobotkiewich, X. Li, J. Shi, I. N. Krivorotov, and S. O. Demokritov, *Sci. Rep.* **8**, 1 (2018).

[10] S. Vélez, J. Schaab, M. S. Wörnle, M. Müller, E. Gradauskaitė, P. Welter, C. Gutgsell, C. Nistor, C. L. Degen, M. Trassin, M. Fiebig, and P. Gambardella, *Nat. Commun.* **10**, 1 (2019).

[11] N. Rohling, E. L. Fjærbu, and A. Brataas, *Phys. Rev. B* **97**, 115401 (2018).

[12] E. L. Fjærbu, N. Rohling, and A. Brataas, *Phys. Rev. B* **100**, 125432 (2019).

[13] E. Erlandsen, A. Kamra, A. Brataas, and A. Sudbø, *Phys. Rev. B* **100**, 100503 (2019).

[14] E. Thingstad, E. Erlandsen, and A. Sudbø, *Phys. Rev. B* **104**, 014508 (2021).

[15] K. Mæland and A. Sudbø, [arXiv:2211.05129](https://arxiv.org/abs/2211.05129).

[16] B. Brekke, A. Sudbø, and A. Brataas, [arXiv:2301.07909](https://arxiv.org/abs/2301.07909).

[17] X. Gong, M. Kargarian, A. Stern, D. Yue, H. Zhou, X. Jin, V. M. Galitski, V. M. Yakovenko, and J. Xia, *Sci. Adv.* **3**, e1602579 (2017).

[18] Ø. Johansen, A. Kamra, C. Ulloa, A. Brataas, and R. A. Duine, *Phys. Rev. Lett.* **123**, 167203 (2019).

[19] A. A. Serga, A. V. Chumak, and B. Hillebrands, *J. Phys. D: Appl. Phys.* **43**, 264002 (2010).

[20] D. Meng, H. Guo, Z. Cui, C. Ma, J. Zhao, J. Lu, H. Xu, Z. Wang, X. Hu, Z. Fu, R. Peng, J. Guo, X. Zhai, G. J. Brown, R. Knize, and Y. Lu, *Proc. Natl. Acad. Sci. U.S.A.* **115**, 2873 (2018).

[21] T. Jungwirth, X. Marti, P. Wadley, and J. Wunderlich, *Nat. Nanotechnol.* **11**, 231 (2016).

[22] C. Sun, H. Yang, and M. B. A. Jalil, *Phys. Rev. B* **105**, 104407 (2022).

[23] A. Kamra, E. Thingstad, G. Rastelli, R. A. Duine, A. Brataas, W. Belzig, and A. Sudbø, *Phys. Rev. B* **100**, 174407 (2019).

[24] E. Erlandsen, A. Brataas, and A. Sudbø, *Phys. Rev. B* **101**, 094503 (2020).

[25] M. Sigrist and K. Ueda, *Rev. Mod. Phys.* **63**, 239 (1991).

[26] K. Fossheim and A. Sudbø, *Superconductivity: Physics and Applications* (Wiley, Chichester, England, 2004).

[27] E. J. Samuels, M. T. Hutchings, and G. Shirane, *Physica* **48**, 13 (1970).

[28] Y. Kajiwara, K. Harii, S. Takahashi, J. Ohe, K. Uchida, M. Mizuguchi, H. Umezawa, H. Kawai, K. Ando, K. Takanashi, S. Maekawa, and E. Saitoh, *Nature* **464**, 262 (2010).

[29] K. Mæland, H. I. Røst, J. W. Wells, and A. Sudbø, *Phys. Rev. B* **104**, 125125 (2021).